Acta Crystallographica Section F
Structural Biology and Crystallization Communications
ISSN 1744-3091

Crystallization and preliminary crystallographic analysis of maganese(II)-dependent 2,3-dihydroxybiphenyl 1,2-dioxygenase from *Bacillus* sp. JF8

Miki Senda,[a] Takashi Hatta,[b] Kazuhide Kimbara[c] and Toshiya Senda[d]*

[a]Structure Guided Drug Development Project, Research and Development Department, Japan Biological Informatics Consortium (JBIC), 2-4-7 Aomi, Koto-ku, Tokyo 135-0064, Japan, [b]Department of Biomedical Engineering, School of Engineering, Okayama University of Science, 1-1 Ridai-cho, Kita-ku, Okayama 700-0005, Japan, [c]Research Institute for Bioresources, Okayama University, 2-20-1 Chuo, Kurashiki, Okayama 710-0046, Japan, and [d]Biomedicinal Information Research Center (BIRC), National Institute of Advanced Industrial Science and Technology (AIST), 2-4-7 Aomi, Koto-ku, Tokyo 135-0064, Japan

Correspondence e-mail: toshiya-senda@aist.go.jp

Received 30 November 2009
Accepted 17 December 2009

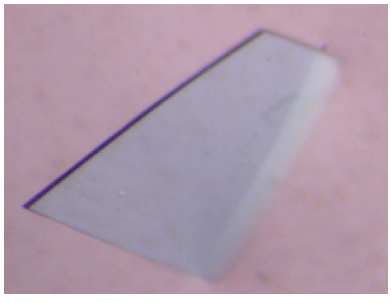

A thermostable manganese(II)-dependent 2,3-dihydroxybiphenyl-1,2-dioxygenase derived from *Bacillus* sp. JF8 was crystallized. The initial screening for crystallization was performed by the sitting-drop vapour-diffusion method using a crystallization robot, resulting in the growth of two crystal forms. The first crystal belonged to space group *P*1, with unit-cell parameters $a = 62.7$, $b = 71.4$, $c = 93.6$ Å, $\alpha = 71.2$, $\beta = 81.0$, $\gamma = 64.0^\circ$, and diffracted to 1.3 Å resolution. The second crystal belonged to space group *I*222, with unit-cell parameters $a = 74.2$, $b = 90.8$, $c = 104.3$ Å, and diffracted to 1.3 Å resolution. Molecular-replacement trials using homoprotocatechuate 2,3-dioxygenase from *Arthrobacter globiformis* (28% amino-acid sequence identity) as a search model provided a satisfactory solution for both crystal forms.

1. Introduction

Aromatic compounds are among the most abundant carbon sources on earth. Since the decomposition of aromatic compounds is essential to the terrestrial carbon cycle, the enzymes that are involved in this cycle have been intensively studied. Type I extradiol dioxygenases (hereafter referred to as extradiol dioxygenases), which catalyze a ring-opening reaction through the addition of two O atoms to the aromatic rings of catechols, are key enzymes in the degradation pathways of aromatic compounds (Lipscomb & Orville, 1992; Vaillancourt *et al.*, 2006). Since extradiol dioxygenases have also been found in the degradation pathways of environmental pollutants such as polychlorinated biphenyls (PCBs; Fukuda, 1993), they have attracted the attention of many researchers.

Extradiol dioxygenases typically contain a nonhaem iron(II) ion in the active site, although some extradiol dioxygenases contain a manganese(II) ion. Since the iron(II) [or manganese(II)] ion is essential to the catalytic reaction of extradiol dioxygenases, the functional role of the iron(II) ion in the catalytic reaction has been of major interest in studies of extradiol dioxygenases. The crystal structures of extradiol dioxygenase BphC derived from *Acidovorax* sp. strain KKS102 (hereafter referred to as BphC_KKS102; Sugiyama *et al.*, 1995; Senda *et al.*, 1996) and that derived from *Burkholderia xenovorans* LB400 (Han *et al.*, 1995) demonstrated that the nonhaem iron(II) ion in the active site coordinates two histidines (His145 and His209 in BphC_KKS102) and one glutamate (Glu260 in BphC_KKS102). The three amino acids in the coordination sphere are completely conserved in the extradiol dioxygenase family (Eltis & Bolin, 1996; Spence *et al.*, 1996). In addition, mutational analysis suggested that another conserved histidine (His194 in BphC_KKS102) located adjacent to the coordination sphere functions as a catalytic base (Senda *et al.*, 1998).

The catalytic mechanism of dioxygenases has been analyzed on the basis of crystal structures (Vaillancourt, Barbosa *et al.*, 2002; Sato *et al.*, 2002; Kovaleva & Lipscomb, 2007). The crystal structures of the reaction intermediates of BphC_KKS102 suggested a binding site for the oxygen molecule and the functional role of the catalytic histidine (Sato *et al.*, 2002). In 2007, the Lipscomb group determined the crystal structures of the reaction intermediates of an oxygen-binding form, showing that the oxygen molecule (or atoms) binds to the

iron(II) ion in a side-on manner (Kovaleva & Lipscomb, 2007). These analyses revealed the catalytic reaction mechanism of extradiol dioxygenases (Kovaleva & Lipscomb, 2007; Lipscomb, 2008).

Despite these structural and biochemical analyses, engineering applications of these enzymes have been difficult to realise because of the instability of iron(II)-dependent extradiol dioxygenases. Oxidation of the iron(II) ion in the active site occurs not only by oxygen molecules in the environment but also by dissociation of the superoxide during turnover (Vaillancourt, Labbé *et al.*, 2002). The oxidized Fe ion dissociates from the enzyme, leading to enzyme inactivation.

However, the characteristics of manganese(II)-dependent extradiol dioxygenases seem to be more suitable for engineering applications (Boldt *et al.*, 1995; Hatta *et al.*, 2003). Since the manganese(II) ion is tolerant to oxidation, Mn(II)-dependent enzymes are quite stable under aerobic conditions. Crystal structures of manganese(II)-dependent extradiol dioxygenases showed that these enzymes share characteristics of the active-site structure with iron(II)-dependent extradiol dioxygenases (Vetting *et al.*, 2004; Emerson *et al.*, 2008). Biochemical analyses revealed that homoprotocatechuate 2,3-dioxygenase from *Brevibacterium fuscum* (HPCD) and the corresponding enzyme from *Arthrobacter globiformis* (MndD) are active with both manganese(II) and iron(II) ions despite their difference in redox potential (Emerson *et al.*, 2008). These results suggested that the iron(II) ion in other extradiol dioxygenases could be replaced with a manganese(II) ion by changing their ion specificity and that the mechanism of ion specificity would be a key to engineering applications of extradiol dioxygenases.

In order to analyze the mechanism of ion selectivity in extradiol dioxygenases, we initiated high-resolution crystal structure analyses of the iron(II)-dependent dioxygenase BphC_KKS102 and of a manganese(II)-dependent extradiol dioxygenase derived from *Bacillus* sp. JF8 (BphC_JF8; Hatta *et al.*, 2003). A detailed comparison of the coordination spheres of the two enzymes from their high-resolution crystal structures should provide novel insights into the ion specificity of these extradiol dioxygenases. BphC_JF8 is a homotetrameric manganese(II)-dependent extradiol dioxygenase (molecular weight 4 × 36.3 kDa; EC 1.13.11.39). This enzyme is thermostable and shows specificity for 2,3-dihydroxybiphenyl (Hatta *et al.*, 2003). Here, we report the crystallization of BphC_JF8.

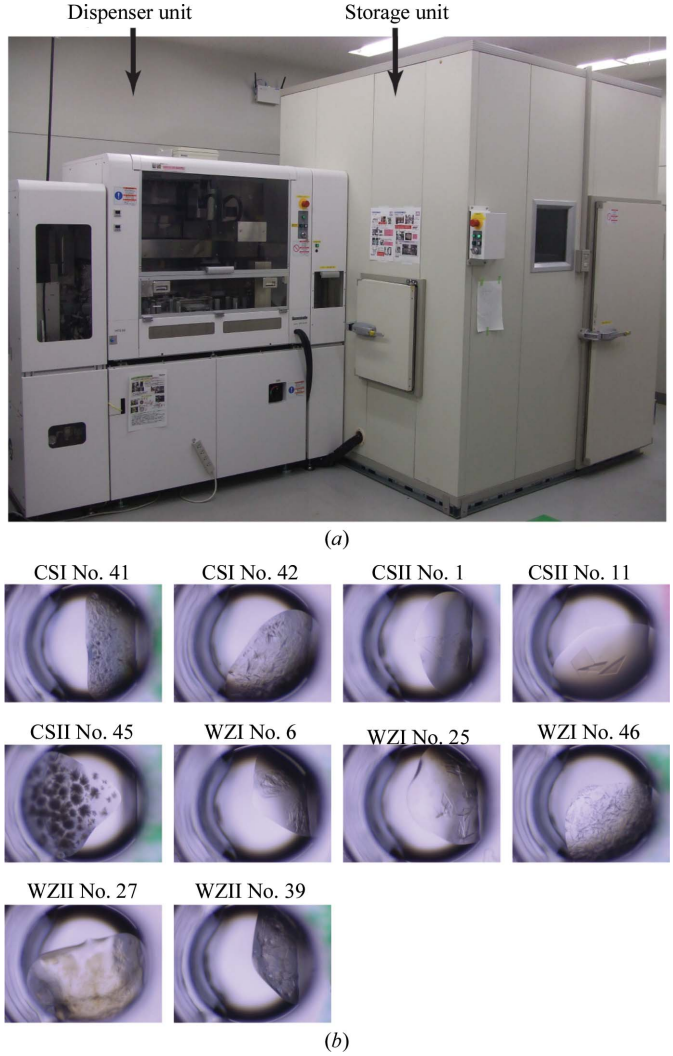

Figure 1
(*a*) HTS-80 crystallization robot (Panasonic) and (*b*) images of the crystals obtained from the initial crystallization screening. CSI, CSII, WZI and WZII represent Crystal Screen I, Crystal Screen II, Wizard I and Wizard II, respectively.

2. Methods and results

2.1. Protein expression, purification and crystallization

BphC_JF8 was overexpressed using *Escherichia coli* MV1190 and purified as described previously (Hatta *et al.*, 2003). Briefly, *E. coli* MV1190 containing plasmid pQW1, which was constructed by inserting the *bphc* gene from *Bacillus* sp. strain JF8 into the pTTQ18 vector (Hatta *et al.*, 2003), was cultured at 333 K for 4 h after IPTG induction. The overexpressed BphC_JF8 was purified by three-step chromatography with DEAE Toyopearl (Tosoh), Phenyl Sepharose HP (GE Healthcare) and Mono Q (GE Healthcare). The purified BphC_JF8 was a manganese(II)-bound form and was concentrated to 75.6 mg ml^{-1} in 50 m*M* Tris–HCl pH 8.0, 10%(*v*/*v*) 2-propanol, 4 m*M* *β*-mercaptoethanol and 1 m*M* manganese(II) chloride.

Initial screening for crystallization was performed by the sitting-drop vapour-diffusion method using an HTS-80 crystallization robot (Panasonic; Miyatake *et al.*, 2005) at 293 K (Fig. 1*a*). A sitting drop was prepared by mixing 1.0 µl each of the protein solution and the reservoir solution and equilibrating the mixture against 50 µl reservoir solution. Crystal Screens I and II (Hampton Research; Jancarik & Kim, 1991) and Wizard I and II (Emerald BioSystems) were used as the reservoir solution. The prepared screening plates were automatically observed and the images of crystallization drops that were obtained were stored on a computer server. Inspection of the images showed that thin plate-like crystals were obtained in 24 h under several conditions: Crystal Screen I Nos. 41 and 42, Crystal Screen II Nos. 1, 11 and 45, Wizard I Nos. 6, 25 and 46 and Wizard II Nos. 27 and 39 (Fig. 1*b*). All reservoir conditions apart from Crystal Screen II No. 11 contained polyethylene glycol (PEG) as a precipitant.

The diffraction quality of these crystals was examined at 100 K using an R-AXIS VII X-ray diffractometer (Rigaku). 1.542 Å in-house Cu $K\alpha$ radiation generated by an FR-E X-ray generator (Rigaku) operated at 45 kV and 45 mA was used for analysis. When a crystal could not be frozen properly in a nitrogen stream, the crystal was soaked in the corresponding reservoir solution containing saturated trehalose for cryoprotection before flash-cooling. A preliminary diffraction study showed that a droplet containing Wizard I condition No. 25 [30%(*v*/*v*) PEG 400, 200 m*M* magnesium chloride, 100 m*M* Tris–HCl pH 8.5] gave the best crystal, which diffracted to approximately 1.8 Å resolution. Therefore, the reservoir conditions of Wizard I condition No. 25 were optimized by changing the PEG 400 concentration from 17.5%(*v*/*v*) to 30.0%(*v*/*v*). When the PEG 400

Table 1
Data-collection statistics.

Values in parentheses are for the outermost resolution shell. A $I/\sigma(I)$ cutoff of −3 was utilized.

			Form II	
	Form I	Form II	Peak	Low remote
Beamline	BL-5A (PF)	BL-5A (PF)	NW-12A (PF-AR)	NW-12A (PF-AR)
Oscillation angle (°)	0.3	1.0	1.0	1.0
Crystal-to-detector distance (mm)	120.0	90.8	75.9	75.0
Exposure time (s)	2	10	2	2
Wavelength (Å)	0.9750	1.0000	1.2822	1.2900
Temperature (K)	100	100	100	100
Space group	*P*1	*I*222	*I*222	*I*222
Unit-cell parameters (Å, °)	a = 62.7, b = 71.4, c = 93.6, α = 71.2, β = 81.0, γ = 64.0	a = 74.2, b = 90.8, c = 104.3	a = 74.2, b = 91.0, c = 104.6	a = 74.2, b = 91.0, c = 104.6
Resolution (Å)	17.0–1.30 (1.36–1.30)	17.0–1.30 (1.36–1.30)	17.0–1.40 (1.47–1.40)	17.0–1.40 (1.47–1.40)
Observations	1019393 (125301)	394502 (50678)	307601 (36185)	316492 (38105)
Unique reflections	319053 (39310)	82688 (10680)	67166 (8977)	67608 (8957)
Completeness (%)	94.0 (91.6)	95.5 (98.6)	96.2 (95.8)	96.9 (95.6)
Redundancy	3.2 (3.2)	4.8 (4.7)	4.6 (4.0)	4.7 (4.3)
Average $I/\sigma(I)$	19.4 (8.0)	19.3 (7.1)	14.9 (4.8)	24.9 (6.0)
$R_{\rm merge}$	0.037 (0.150)	0.050 (0.217)	0.059 (0.289)	0.037 (0.240)
Mosaicity (°)	0.357	0.226	0.170	0.173

concentration in the reservoir solution was increased, the crystal size and thickness were reduced. After several trials, the optimal reservoir conditions were determined to be 18%(*v*/*v*) PEG 400, 100 m*M* Tris–HCl pH 8.5 and 200 m*M* magnesium chloride. Crystallization temperatures of 277 and 293 K were tested; the crystals obtained at 293 K were larger and thicker than those obtained at 277 K. Crystals grew at 293 K to approximate dimensions of 1.0 × 0.5 × 0.03 mm in 1–2 weeks (Fig. 2*a*). These crystals were designated form I.

Approximately 1 year after the initial screening, microcrystals were found in the initial screening plates under several conditions in which low-molecular-weight alcohols such as ethanol, 2-propanol and 1,4-butanediol had been included as a precipitant. Crystallization conditions were thus optimized using 2-propanol [5–20%(*v*/*v*)] or ethanol [5–20%(*v*/*v*)] as a precipitant at pH 6.5 (100 m*M* MES–NaOH) or pH 7.5 (100 m*M* HEPES–NaOH) with 200 m*M* zinc acetate. After optimization of the reservoir conditions, oval-shaped crystals were obtained with a reservoir solution consisting of 10%(*v*/*v*) 2-propanol, 100 m*M* MES–NaOH pH 6.5 and 200 m*M* zinc acetate. Crystals grew at 293 K to approximate dimensions of 0.2 × 0.1 × 0.1 mm in 2–3 d (Fig. 2*b*). These crystals were designated form II.

2.2. X-ray diffraction analysis

Diffraction data were collected at 100 K using an ADSC CCD detector on beamline BL-5A of Photon Factory (PF; KEK, Tsukuba) or on beamline NW-12A of Photon Factory Advanced Ring (PF-AR; KEK, Tsukuba). Prior to data collection, the form I crystal was soaked in a cryoprotectant solution [30%(*v*/*v*) PEG 400, 100 m*M* Tris–HCl pH 8.5 and 200 m*M* magnesium chloride] for 20 s and flash-cooled in liquid nitrogen. The form II crystal was cryoprotected by soaking in 30%(*v*/*v*) glycerol, 10.5%(*v*/*v*) 2-propanol, 70 m*M* MES–NaOH pH 6.5 and 140 m*M* zinc acetate for 2 min and flash-cooled in liquid nitrogen.

The diffraction data were processed and scaled using the programs *XDS* and *XSCALE* (Kabsch, 1993). The form I and form II crystals belonged to space groups *P*1 and *I*222, respectively (Table 1). Both crystals diffracted to approximately 1.3 Å resolution and the data could be processed and scaled with reasonably good results (Table 1). Assuming the presence of four subunits of BphC_JF8 (145.2 kDa) in the asymmetric unit of crystal form I, the Matthews coefficient ($V_{\rm M}$) was calculated to be 2.5 Å^3 Da^{-1}, corresponding to a solvent content of 49.4% (Matthews, 1968). Since BphC_JF8 is a tetrameric enzyme, the asymmetric unit of the form I crystal is likely to contain a whole enzyme. Assuming one subunit of BphC_JF8 (36.3 kDa) per asymmetric unit of crystal form II, the $V_{\rm M}$ value was calculated to be 2.4 Å^3 Da^{-1}, corresponding to a solvent content of 48.8% (Matthews, 1968). The 222 symmetry of tetrameric BphC_JF8 seems to coincide with that of the form II crystal.

Molecular-replacement calculations were performed with the program *MOLREP* (Vagin & Teplyakov, 1997) in the *CCP*4 program suite (Collaborative Computational Project, Number 4, 1994) using

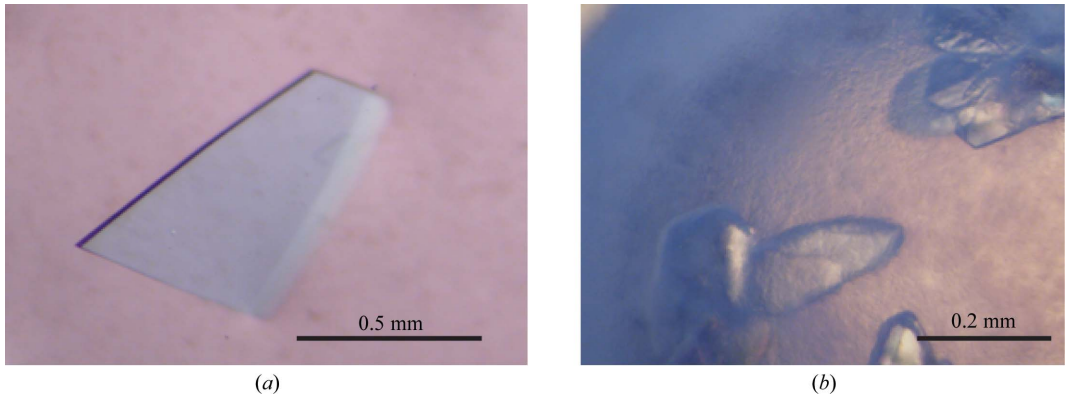

(*a*) (*b*)

Figure 2
(*a*) A form I crystal of BphC_JF8. (*b*) Form II crystals of BphC_JF8.

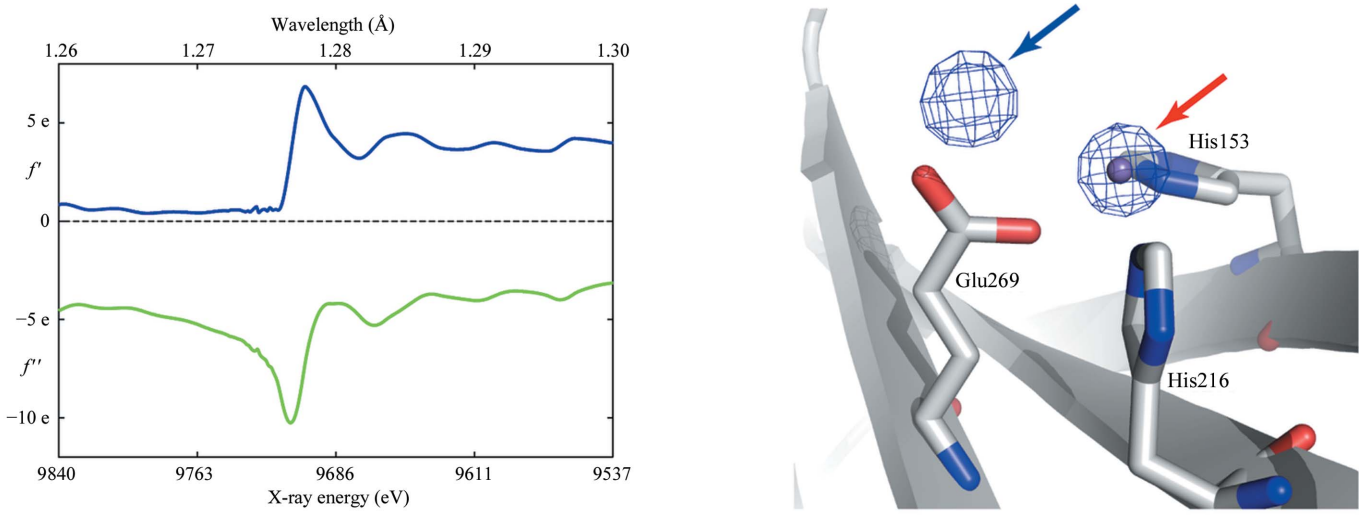

Figure 3
(*a*) The anomalous scattering factors f' and f'' around the absorption edge of Zn were calculated from the fluorescence spectra of a form II crystal using the program *CHOOCH* (Evans & Pettifer, 2001). (*b*) An $F_{\rm peak} - F_{\rm low\ remote}$ difference Fourier map around the active site of a form II crystal. The electron density was contoured at the 10σ level. Red and blue arrows indicate electron densities at the manganese(II) ion site and at its adjacent site, respectively.

homoprotocatechuate 2,3-dioxygenase from *A. globiformis* as the search model (PDB entry 1f1u; Vetting *et al.*, 2004). Satisfactory molecular-replacement solutions were found for both crystal forms. Several cycles of crystallographic refinement with the program *REFMAC*5 (Murshudov *et al.*, 1997) and model building with the program *Coot* (Emsley & Cowtan, 2004) revealed the active-site structure of BphC_JF8. As expected from its primary sequence, two histidines (His153 and His216) and one glutamate (Glu269) coordinate the manganese(II) ion in both crystal forms. However, in form II a strong density was observed adjacent to the manganese(II) ion. Comparison of the crystallization conditions of the two crystal forms suggested that the extra density in the form II crystal represents a Zn ion. Indeed, an X-ray absorption spectrum around the absorption edge of Zn suggested that the form II crystals contained Zn ions (Fig. 3*a*). An $F_{\rm peak} - F_{\rm low\ remote}$ difference Fourier map of a form II crystal at 1.4 Å resolution showed two densities in the active site. One density was located at the same position as the manganese(II) ion and the other density was located at the above-described site adjacent to the manganese(II) ion (Table 1, Fig. 3*b*). This result showed that the coordination sphere of the form II crystal contained two Zn ions. The knowledge accumulated on extradiol dioxygenases suggested that this structure was a crystallographic artifact. We therefore decided to perform high-resolution crystallographic refinement using the diffraction data from the form I crystal. Crystallographic refinement with the program *SHELXL* (Sheldrick, 2008) is in progress.

This study was supported in part by the New Energy and Industrial Technology Development Organization (NEDO) of Japan.

References

Boldt, V. R., Sadowsky, M. J., Ellis, L. B. M., Que, L. Jr & Wackett, L. P. (1995). *J. Bacteriol.* **177**, 1225–1232.
Collaborative Computational Project, Number 4 (1994). *Acta Cryst.* D**50**, 760–763.
Eltis, L. D. & Bolin, J. T. (1996). *J. Bacteriol.* **178**, 5930–5937.
Emerson, J. P., Kovaleva, E. G., Farquhar, E. R., Lipscomb, J. D. & Que, L. Jr (2008). *Proc. Natl Acad. Sci. USA*, **105**, 7347–7352.
Emsley, P. & Cowtan, K. (2004). *Acta Cryst.* D**60**, 2126–2132.
Evans, G. & Pettifer, R. F. (2001). *J. Appl. Cryst.* **34**, 82–86.
Fukuda, M. (1993). *Curr. Opin. Biotechnol.* **4**, 339–343.
Han, S., Eltis, L. D., Timmis, K. N., Muchmore, S. W. & Bolin, J. T. (1995). *Science*, **270**, 976–980.
Hatta, T., Mukerjee-Dhar, G., Damborsky, J., Kiyohara, H. & Kimbara, K. (2003). *J. Biol. Chem.* **278**, 21483–21492.
Jancarik, J. & Kim, S.-H. (1991). *J. Appl. Cryst.* **24**, 409–411.
Kabsch, W. (1993). *J. Appl. Cryst.* **26**, 795–800.
Kovaleva, E. G. & Lipscomb, J. D. (2007). *Science*, **316**, 453–457.
Lipscomb, J. D. (2008). *Curr. Opin. Struct. Biol.* **18**, 644–649.
Lipscomb, J. D. & Orville, A. M. (1992). *Met. Ions Biol. Syst.* **28**, 243–293.
Matthews, B. W. (1968). *J. Mol. Biol.* **33**, 491–497.
Miyatake, H., Kim, S.-H., Motegi, I., Matsuzaki, H., Kitahara, H., Higuchi, A. & Miki, K. (2005). *Acta Cryst.* D**61**, 658–663.
Murshudov, G. N., Vagin, A. A. & Dodson, E. J. (1997). *Acta Cryst.* D**53**, 240–255.
Sato, N., Uragami, Y., Nishizaki, T., Takahashi, Y., Sazaki, G., Sugimoto, K., Nonaka, T., Masai, E., Fukuda, M. & Senda, T. (2002). *J. Mol. Biol.* **321**, 621–636.
Senda, T., Sugimoto, K., Nishizaki, T., Okano, M., Yamada, T., Masai, E., Fukuda, M. & Mitsui, Y. (1998). *Oxygen Homeostasis and its Dynamics*, edited by Y. Ishimura, H. Shimada & M. Suematsu, pp 276–281. Tokyo: Springer-Verlag.
Senda, T., Sugiyama, K., Narita, H., Yamamoto, T., Kimbara, K., Fukuda, M., Sato, M., Yano, K. & Mitsui, Y. (1996). *J. Mol. Biol.* **255**, 735–752.
Sheldrick, G. M. (2008). *Acta Cryst.* A**64**, 112–122.
Spence, E. L., Kawamukai, M., Sanvoisin, J., Braven, H. & Bugg, T. D. H. (1996). *J. Bacteriol.* **178**, 5249–5256.
Sugiyama, K., Senda, T., Narita, H., Yamamoto, T., Kimbara, K., Fukuda, M., Yano, K. & Mitsui, M. (1995). *Proc. Jpn Acad. Ser. B Phys. Biol. Sci.* **71**, 33–35.
Vagin, A. & Teplyakov, A. (1997). *J. Appl. Cryst.* **30**, 1022–1025.
Vaillancourt, F. H., Barbosa, C. J., Spiro, T. G., Bolin, J. T., Blades, M. W., Turner, R. F. B. & Eltis, L. D. (2002). *J. Am. Chem. Soc.* **124**, 2485–2496.
Vaillancourt, F. H., Bolin, J. T. & Eltis, L. D. (2006). *Crit. Rev. Biochem. Mol. Biol.* **41**, 241–267.
Vaillancourt, F. H., Labbé, G., Drouin, N. M., Fortin, P. D. & Eltis, L. D. (2002). *J. Biol. Chem.* **277**, 2019–2027.
Vetting, M. W., Wackett, L. P., Que, L. Jr, Lipscomb, J. D. & Ohlendorf, D. H. (2004). *J. Bacteriol.* **186**, 1945–1958.